ECCOMAS Congress 2016
VII European Congress on Computational Methods in Applied Sciences and Engineering
M. Papadrakakis, V. Papadopoulos, G. Stefanou, V. Plevris (eds.)
Crete Island, Greece, 5–10 June 2016

# APPLICATION OF WHIRL FLUTTER OPTIMIZATION-BASED SOLUTION TO FULL-SPAN MODEL OF TWIN TURBOPROP AIRCRAFT

**Jiri Cecrdle**[1]

[1] Aeronautical Research and Test Institute
Beranovych 130, Prague, Czech Republic
e-mail: cecrdle@vzlu.cz

**Keywords:** Flutter, Whirl Flutter, Optimization, L-410NG aircraft.

**Abstract.** *This paper deals with whirl flutter analysis of aircraft structures. It gives the theoretical background of the whirl flutter phenomenon and aircraft certification-related issues. After that, the ordinary and optimization-based analytical approaches are described. The optimization based analytical procedure is used to determine the whirl flutter stability boundaries for the certification speed. The focus is on the application of the optimization-based approach on a full-span model of an aircraft structure. The necessary adjustments of a stick computational model to make it applicable as a full-span and also the modification of the optimization solution are described. The methodology is demonstrated on the model of a twin-engine turboprop commuter aircraft. The evaluated results include the available choices of both propeller rotation directions, i.e. CW-CW and CW-CCW. Finally, the outlook and the future work on the described topic is outlined.*

## 1 INTRODUCTION

Turboprop aircraft are certified considering the whirl flutter stability. Whirl flutter is a specific type of flutter instability caused by the effect of rotating parts as a propeller or a gas turbine engine rotor. Rotating mass causes additional forces and moments and increases the number of degrees-of-freedom. Rotating propeller also causes aerodynamic interference effect with a nacelle and a wing structure. Whirl flutter instability is driven by motion-induced unsteady aerodynamic propeller forces and moments acting in the propeller plane. It is quite serious phenomenon, that may cause unstable vibration of a propeller mounting, even a failure of an engine installation or a whole wing. Airworthiness regulations require flutter analysis taking into account the influence of the degrees of freedom of the propeller plane of rotation and significant elastic, inertia and aerodynamic forces. Also the changes in the stiffness and damping of the propeller–engine–nacelle structure system must be considered (FAR/CS §23.629(e)(1)(2)) [1, 2].

The reliable stiffness data regarding the engine attachment are not usually at disposal until the ground vibration test of the prototype is done and the final updating of the analytical model is possible. Nevertheless, considering timesaving in the final development phase, it is worth performing whirl flutter calculations in the earlier phase. For this purpose, an optimization based analytical procedure to determine the critical values of an engine attachment stiffness parameters was prepared. It allows determination of whirl flutter and whirl divergence stability boundaries for the speed, which is set by regulations as the certification speed. The solution employs the gradient-based algorithm and includes modal-based and flutter-based design responses. Design variables are represented by the engine attachment stiffness parameters.

The initial solution was prepared for the half-span models of aircraft with either symmetric or antisymmetric boundary condition, which are usually used for flutter analyses. But, the applicability of half-span models is limited and application of a full-span model is necessary in some cases. The typical example is the whirl flutter. Considering the usual twin wing-mounted engine aircraft concept, one of the parameters influencing the whirl flutter stability is the direction of rotation of both propellers. Therefore, the applicability of the optimization-based solution was enlarged also to the full-span models. The optimization solution for a full-span model is, compare to a half-span model, more complicated. Also, the specific adjustment of a structural model is necessary. The solution is demonstrated on the example of the reference model of the twin-engine turboprop commuter aircraft. Whirl flutter stability boundaries are constructed for different conditions of propeller rotations.

## 2 THEORETICAL BACKGROUND

The principle of whirl flutter phenomenon is outlined on the simple mechanical system with two degrees-of-freedom. Propeller and hub are considered as rigid. An engine flexible mounting is represented by two rotational springs (stiffness $K_\Psi$, $K_\Theta$) as illustrated in figure 1. Such a system has two independent mode shapes (yaw and pitch) with angular frequencies $\omega_\Psi$ and $\omega_\Theta$. Considering a propeller rotation with the angular velocity $\Omega$, the primary motion changes and the gyroscopic effect makes both independent mode shapes merge into the whirl motion. A propeller axis of rotation shows an elliptical movement. A trajectory of this elliptical movement depends on both angular frequencies $\omega_\Psi$ and $\omega_\Theta$. The orientation of the gyroscopic movement is backward relative to the propeller rotation for the mode with the lower frequency (backward whirl mode) and forward relative to the propeller rotation for the mode with the higher frequency (forward whirl mode). Because the yaw and pitch motions have a 90° phase shift, the mode shapes in the presence of gyroscopic effects are complex.

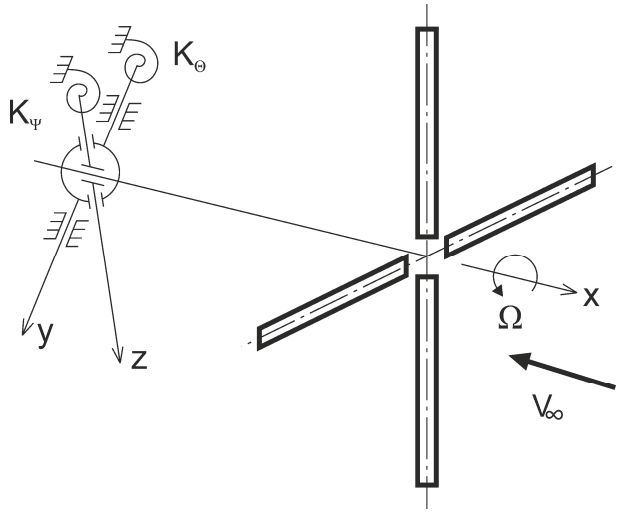


Figure 1. Gyroscopic system with propeller.

The gyroscopic motion results in changes of the propeller blades' angles of attack and consequently, leading to unsteady aerodynamic forces. These forces may under specific conditions induce whirl flutter instability. The flutter state is defined as the neutral stability with no damping of the system and the corresponding airflow ($V_\infty = V_{FL}$) is called critical flutter speed. If the air velocity is lower than flutter speed ($V_\infty < V_{FL}$), the system is stable and the gyroscopic motion is damped (see figure 2a). If the airspeed exceeds the flutter speed ($V_\infty > V_{FL}$), the system becomes unstable, and gyroscopic motion divergent (see figure 2b).

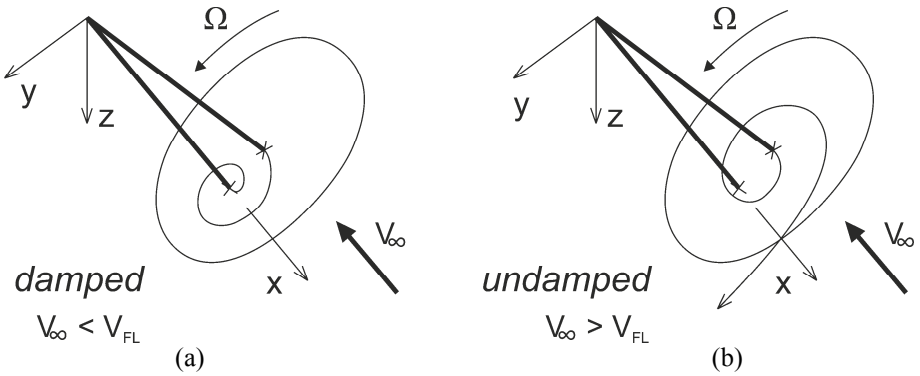


Figure 2. Stable (a) and unstable (b) state of gyroscopic vibrations for backward flutter mode.

The analytical solution is aimed to determine the aerodynamic force caused by the gyroscopic motion on each of propeller blades. Presented equations of motion were derived for the system shown in figure 1 using Lagrange's approach. The kinematical scheme is shown in figure 3. We select three angles ($\varphi$, $\Theta$, $\Psi$) as the independent generalised coordinates. The propeller angular velocity is considered constant ($\varphi = \Omega\, t$). The rotating part is assumed cyclically symmetric with respect to both mass and aerodynamics (i.e., propeller of three blades in minimum). Non-uniform mass moments of inertia of the engine with respect to pitch and yaw axes ($J_Z \neq J_Y$) are considered.

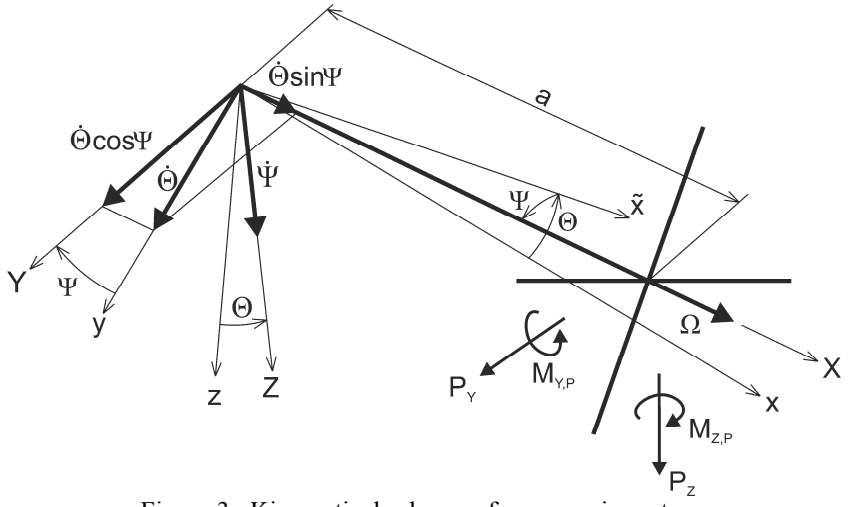


Figure 3. Kinematical scheme of gyroscopic system.

Considering small angles, the equations of motion become:

$$\begin{aligned} J_Y\ddot{\Theta} + \frac{K_\Theta \gamma_\Theta}{\omega}\dot{\Theta} + J_X \Omega \dot{\Psi} + K_\Theta \Theta &= M_{Y,P} - a.P_Z \\ J_Z\ddot{\Psi} + \frac{K_\Psi \gamma_\Psi}{\omega}\dot{\Psi} - J_X \Omega \dot{\Theta} + K_\Psi \Psi &= M_{Z,P} + a.P_Y \end{aligned} \tag{1}$$

where a is the distance between a propeller plane and a vibration mode node point. Neglecting the aerodynamic inertia terms ( $\dot{\Theta}^* \approx \dot{\Theta}$ ; $\dot{\Psi}^* \approx \dot{\Psi}$ ), the propeller aerodynamic forces and moments at the propeller plane ($P_Y$; $P_Z$; $M_{Y,P}$; $M_{Z,P}$) are calculated as:

$$\begin{aligned} P_Y &= \pi\,\rho\,V_\infty^2 R^2 \left( c_{y\Theta}\Theta^* + c_{y\Psi}\Psi^* + c_{yq}\frac{\dot{\Theta}^* R}{V_\infty} + c_{yr}\frac{\dot{\Psi}^* R}{V_\infty} \right) \\ P_Z &= \pi\,\rho\,V_\infty^2 R^2 \left( c_{z\Theta}\Theta^* + c_{z\Psi}\Psi^* + c_{zq}\frac{\dot{\Theta}^* R}{V_\infty} + c_{zr}\frac{\dot{\Psi}^* R}{V_\infty} \right) \\ M_{Y,P} &= 2\pi\,\rho\,V_\infty^2 R^3 \left( c_{m\Theta}\Theta^* + c_{m\Psi}\Psi^* + c_{mq}\frac{\dot{\Theta}^* R}{V_\infty} + c_{mr}\frac{\dot{\Psi}^* R}{V_\infty} \right) \\ M_{Z,P} &= 2\pi\,\rho\,V_\infty^2 R^3 \left( c_{n\Theta}\Theta^* + c_{n\Psi}\Psi^* + c_{nq}\frac{\dot{\Theta}^* R}{V_\infty} + c_{nr}\frac{\dot{\Psi}^* R}{V_\infty} \right) \end{aligned} \tag{2}$$

where ρ is an air density and R is a propeller radius. Aerodynamic derivatives (c-terms) are given from the propeller blade integrals (by [3, 4] or by [5]). Using the quasi-steady theory [6], the effective angles ($\Theta^*$, $\Psi^*$) become:

$$\begin{aligned} \Theta^* &= \left( \Theta + \frac{\dot{z}}{V_\infty} \right) - \frac{w_1}{V_\infty} \\ \Psi^* &= \left( \Psi - \frac{\dot{y}}{V_\infty} \right) + \frac{w_2}{V_\infty} \end{aligned} \tag{3}$$

where ($w_1/V_\infty$) and ($w_2/V_\infty$) are optional downwash and sidewash terms. Downwash and sidewash angles behind the propeller describe the interference between propeller and nacelle.

Induced downwash and sidewash angles are added to the effective static angles, which are represented by the remaining terms of eq. (3). Induced downwash and sidewash angles, which are dependent on the reduced frequency, can be obtained from the lift solution by partitioning the interference coefficients. The downwash effect influences the aerodynamic stiffness matrix; the influence to the aerodynamic damping matrix is neglected. An option to include the downwash and sidewash effects may be important for the aircraft configuration with wing-mounted engines.

Finally, seeking for the critical (flutter) state assuming the harmonic motion has a character of an eigenvalue problem. The final whirl flutter matrix equation can be expressed as:

$$\left(-\omega^2[M]+j\omega\left([D]+[G]+q_\infty\frac{4\pi R^4}{V_\infty}[D^A]\right)+\left([K]+q_\infty 2\pi R^3[K^A]\right)\right)\begin{bmatrix}\overline{\Theta}\\ \overline{\Psi}\end{bmatrix}=\{0\} \tag{4}$$

where [M] is mass matrix, [D] is structural damping matrix, [K] is structural stiffness matrix. $[D^A]$ and $[K^A]$ are aerodynamic damping and aerodynamic stiffness matrix, respectively. Finally, [G] is gyroscopic matrix. The critical state emerges when the angular velocity ω is real. The critical state can be reached by increasing either $V_\infty$ or Ω. Increasing the propeller advance ratio ($V_\infty$ / (ΩR)) has destabilizing effect. Another important parameter is distance of propeller plane and node points of engine vibration modes. Structural damping is a significant stabilization factor. The paper [7] describes an experiment during which friction was deeply suppressed and whirl flutter occurred. However, the notably slight structural damping made the model stable. By contrast, the influence of the propeller thrust is negligible. This small influence comes from the fact that the aerodynamic derivatives of the thrusted propeller and windmilling propeller variance can be high in the low speed region, but at high velocities (where whirl flutter is expected), the variance is less than 5% [8]. The most critical state is $\omega_\Theta = \omega_\Psi$ when the interaction of both independent motions is maximal and the trajectory of the gyroscopic motion is circular. Considering the rigid propeller blades, the whirl flutter inherently appears at the backward gyroscopic mode. A special case of eq. (4) for $\omega = 0$ is gyroscopic static divergence, which is characteristic by uni-directional divergent motion.

The described model that considers a rigid propeller is obviously applicable to conventional propellers, for which the propeller blade frequencies are much higher compared to the nacelle pitch and yaw frequencies. Considering the large multi-bladed propellers of heavy turboprop aircraft, the consideration of a rigid propeller appears too conservative and the blade flexibility must also be modeled. Obviously, the whirl flutter investigation of tilt-rotor aircraft must include even more complex analytical models [9].

The comprehensive information regarding the whirl flutter phenomenon can be found in [10].

## 3 STANDARD ANALYTICAL APPROACH

The standard whirl flutter solution is based on the strip aerodynamic theory [11] for the propeller at the windmilling mode. The propeller is assumed rigid. For the residual structure the unsteady doublett-lattice method including wing–body interference aerodynamic theory is used [12]. For the flutter stability solution the p-k method [13] is applied. The basic flutter equation in modal coordinates is:

$$\left[[M_{hh}]\lambda^2+\left([B_{hh}]-\frac{1}{4}\rho\,\bar{c}\,V_\infty\frac{[Q_{hh}^{\mathrm{Im}}]}{k}\right)\lambda+\left([K_{hh}]-\frac{1}{2}\rho\,V_\infty^2\,[Q_{hh}^{\mathrm{Re}}]\right)\right]\{u_h\}=0 \tag{5}$$

$[M_{hh}]$, $[B_{hh}]$ and $[K_{hh}]$ are modal mass, damping and stiffness matrices, respectively, a function of the Mach number (M) and the reduced frequency (k). Aerodynamic loads are incorporated into damping and stiffness matrices. $[Q_{hh}^{Re}]$ and $[Q_{hh}^{Im}]$ are the real and the imaginary part of a complex aerodynamic matrix, also a function of parameters M and k. The parameter $\rho$ is the air density, $\overline{c}$ is a reference length, and $\{u_h\}$ is a modal amplitude vector. The eigenvalue $\lambda$ is given as:

$$\lambda = \omega\left(\gamma \pm j\right) \tag{6}$$

and $\gamma$ is a transient decay rate coefficient. Note that the structural damping coefficient (g) is expressed as:

$$g = 2.\gamma \tag{7}$$

The standard whirl flutter solution is performed for multiple velocities. The resulting quantities are V-g-f curves, i.e. the dependence of the damping and frequency of analyzed modes on the flight velocity. The state with the zero damping represents the critical flutter state and the corresponding flight velocity is the critical flutter speed.

## 4 OPTIMIZATION-BASED ANALYTICAL APPROACH

Optimization-based approach employs the gradient-based algorithms [14] for the whirl flutter solution. It makes possible the calculation of the flutter stability boundaries for the specified certification speed. In this case, the flutter speed is set equal to the certification speed, and the results are critical values of the structural parameters. The stability margin can be then obtained from these critical structural parameters. The analyzed states are then compared only with respect to the structural parameters and the relationship to the stability margin. Such an approach can save large amounts of time because the number of whirl flutter analyses required by the regulations is dramatically reduced.

The whirl flutter optimization employs two types of the design responses (eigenvalue and flutter). The eigenvalue equation is:

$$\left(\left[K\right]-\lambda_n\left[M\right]\right)\left\{\phi_n\right\}=0 \tag{8}$$

where $\lambda_n$ and $\phi_n$ are the $n^{th}$ eigenvalue and eigenvector, respectively. [K] is the structural stiffness and [M] is the structural mass matrix. Eq. (8) can be differentiated with respect to the $i^{th}$ design variable $x_i$:

$$\left(\left[K\right]-\lambda_n\left[M\right]\right)\frac{\partial\left\{\phi_n\right\}}{\partial x_i}+\left(\frac{\partial\left[K\right]}{\partial x_i}-\lambda_n\frac{\partial\left[M\right]}{\partial x_i}\right)\left\{\phi_n\right\}=\frac{\partial\lambda_n}{\partial x_i}\left[M\right]\left\{\phi_n\right\} \tag{9}$$

When eq. (9) is premultiplied by $\phi_n^T$, the first term becomes zero and eq. (9) can then be solved for the eigenvalue derivatives:

$$\frac{\partial\lambda_n}{\partial x_i}=\frac{\left\{\phi_n\right\}^T\left(\frac{\partial\left[K\right]}{\partial x_i}-\lambda_n\frac{\partial\left[M\right]}{\partial x_i}\right)\left\{\phi_n\right\}}{\left\{\phi_n\right\}^T\left[M\right]\left\{\phi_n\right\}} \tag{10}$$

In practice, the solution of eq. (10) is based on the semi-analytical approach. The derivatives of the mass and stiffness matrices are approximated using the finite differences.

The equation is solved for each retained eigenvalue referenced in the design model and for each design variable.

Aeroelastic flutter stability matrix equation is given by eq. (5). The equation represents the p-k method of the flutter solution, which is the only method applicable for the purpose of the design optimization. Flutter sensitivity computes the rates of change of the transient decay rate coefficient $\gamma$ with respect to changes of the design variables. Eq. (5) is differentiated with respect to the design variables for the quantity $(\partial\gamma/\partial x_i)$. The solution is semi-analytical in nature with derivatives approximated using either forward differences or central differences.

Flutter sensitivities are computed as the rate of change of the transient decay coefficient $\gamma$ with respect to changes in design variables $(\partial\gamma/\partial x_i)$.

The optimization-based whirl flutter solution is performed for a single velocity. The resulting quantities are structural parameters, for which the flutter speed is equal to the specified certification speed.

## 5 STRUCTURAL MODEL OF AIRCRAFT STRUCTURE

### 5.1 Half-span Model

Aeroelastic analyses of aircraft structures are usually performed using simple dynamic structural models (stick models). Stiffness characteristics of the structural parts are modeled by means of the massless beam elements, and inertial characteristics are modeled by concentrated mass elements including appropriate moments of inertia. The model also includes spring elements, various conditions and auxiliary elements (controls suspension, visualization, etc.). In the most cases, the analysis can be performed using half-span model. In this case, the half-values of the stiffness and inertial characteristics are applied at the plane of symmetry as well as either symmetric or antisymmetric boundary condition. Such a model is shown in figure 4. Attachment of the engine to the wing is realized simply by means of two spring elements, which model engine pitch and yaw vibration modes. Stiffness constant of the spring determines the natural frequency of the mode. Spring element is stationed at the node point of the mode.

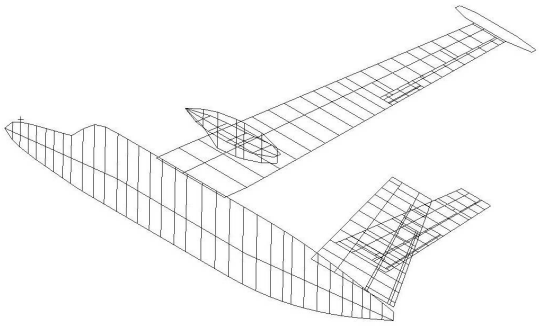

Figure 4. Half-span structural model of twin engine turboprop commuter aircraft.

## 5.2 Full-span Model

The applicability of half-span models is limited and application of a full-span model is necessary in some specific cases. In the case of the full-span model, both symmetric and antisymmetric engine vibration modes must be modeled. Such a model is shown in figure 5.

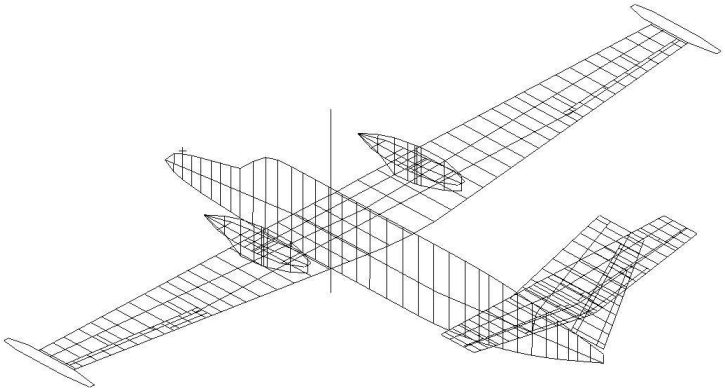

Figure 5. Full-span structural model of twin engine turboprop commuter aircraft.

The engine attachment includes four modes with diverse natural frequencies and diverse node points. The typical order of engine modes (by frequency) is 1) symmetric pitch, 2) symmetric yaw, 3) antisymmetric pitch and, 4) antisymmetric yaw. The node points of these modes are typically stationed in the direction from the rear to the front (in the flight direction).

The systems to model pitch and yaw engine vibration modes are separate. The appropriate rotational degree-of-freedom (i.e., around lateral or around vertical axis) is connected to the central system, which consists of the grounded spring element and two rod elements. The grounded spring is placed at the plane of symmetry at the station of the node of the symmetric mode while rod elements are placed at the station of the node point of the antisymmetric mode. Rod elements are oriented in the appropriate direction (i.e., laterally or vertically). Node point of the grounded spring is connected with the central node of rod elements by means of multi-point constraint. Apart from the appropriate degree-of-freedom, other ones are omitted from the analysis. Spring constant of the grounded spring element $K_\delta$ and the torsional stiffness of rod elements ($GI_k$) then determine natural frequencies of both symmetric and antisymmetric mode. Spring constant is decisive for the symmetric mode frequency, while rod torsional stiffness is decisive for the antisymmetric frequency. However, there is also cross-influence; and therefore, both parameters must be used to set both frequencies. The examples of mentioned engine vibration modes are shown in figure 6.

Note, that also both symmetric and antisymmetric control surface and tab flapping modes must be modeled on the full-span models. However, no detailed description of the modeling technique is provided here as these modes are not important from the whirl flutter phenomenon point of view.

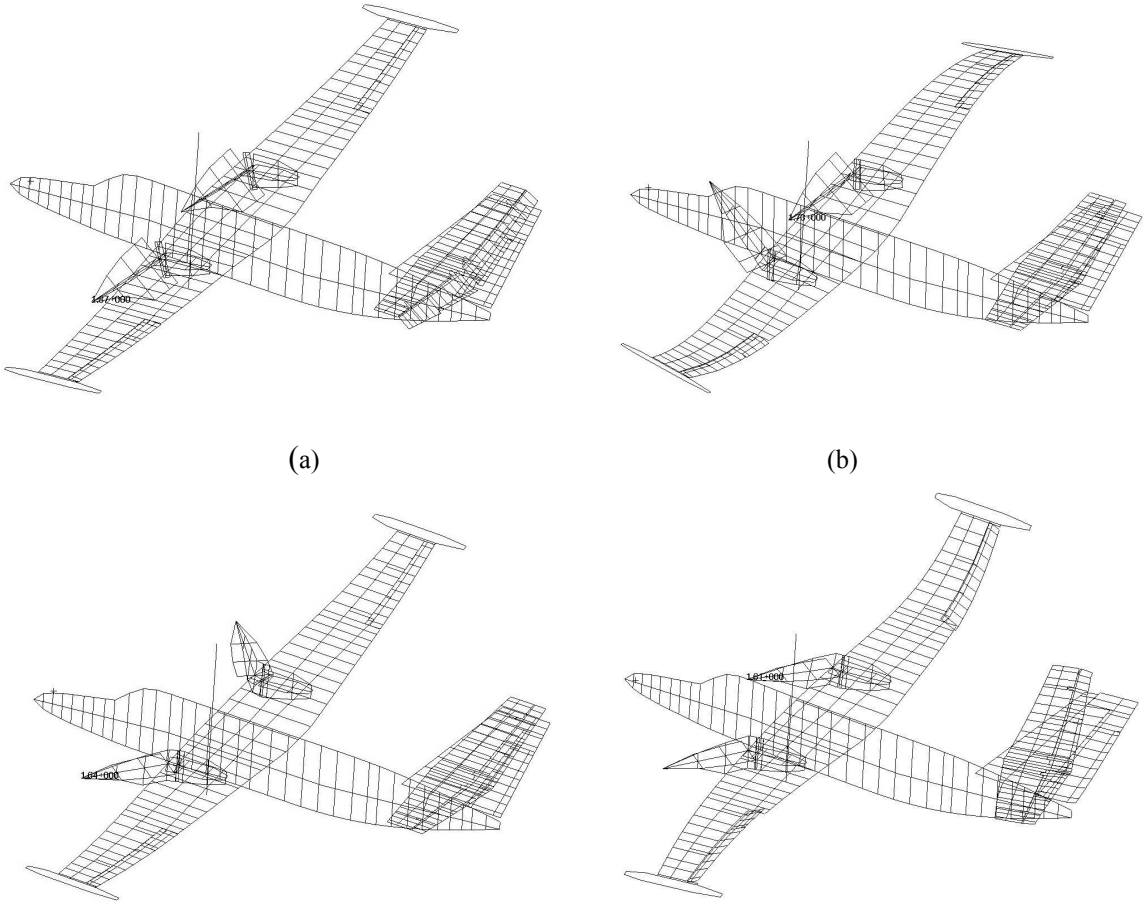

(a) (b)

(c) (d)

Figure 6. Engine vibration modes: (a) symmetric pitch, (b) antisymmetric pitch, (c) symmetric yaw, (d) antisymmetric yaw.

## 6 DESCRIPTION OF OPTIMIZATION-BASED SOLUTION

The important parameters influencing the whirl flutter stability are engine pitch and yaw frequencies. The solution is therefore demonstrated on the example of variation of these parameters. We consider the inertia characteristics of the engine and propeller system as well as the characteristics of the residual structure to be reliably determined; thus, we will use the engine attachment stiffness properties as parameters for the optimization.

### 6.1 Solution for Half-span Model

We define two design variables: 1) effective stiffness of the engine attachment in pitch and 2) effective stiffness of the engine attachment in yaw. These design variables are directly related to the spring constants of two spring elements (pitch-$K_{\varphi V}$ and yaw-$K_{\varphi H}$ ).

The first preparatory step is intended to set the initial design variables for the main optimization. The target frequency ratio (TFR) is set, and both effective stiffnesses are adjusted to reach this target ratio. The simplest way is to set any of the mentioned stiffnesses as the design variable (while the other one is fixed) and use the optimization solution with the objective function (OBJ) defined as:

$$OBJ = min\left[ ABS\left( \frac{f_2}{f_1} - TFR \right) \right] \tag{11}$$

where ABS denotes for the absolute value. Symbols $f_1$ and $f_2$ represent both pitch and yaw engine frequencies ($f_2$ is the higher frequency while $f_1$ is the lower frequency). Note that the yaw frequency is usually higher compare to the pitch frequency; nevertheless, the solution may be done regardless the frequency order. This preparatory analysis gives the initial values of $K_{\varphi V}$ and $K_{\varphi H}$ for the main optimization. The ratio of both frequencies (pitch-$f_\Theta$ and yaw-$f_\Psi$) is equal to the TFR.

The main optimization includes both design variables ($K_{\varphi V}$ and $K_{\varphi H}$). The design constraints include the requirement to keep the target frequency ratio. For the practical applications, specification of a constraint with the ±2% band is usually used:

$$ABS\left(\frac{\left(\frac{f_2}{f_1}-TFR\right)}{TFR}\right)<0.02 \tag{12}$$

Another constraint includes the requirement to keep the flutter stability (i.e., negative damping) at the selected certification speed $V_{cert}$. This requirement is expressed as:

$$g\left(V=V_{cert}\right)<0 \tag{13}$$

In the practical solution, the constraint is modified as:

$$-\infty<\left(\frac{g\left(V=V_{cert}\right)-0.03}{0.1}\right)<-0.3 \tag{14}$$

The interval shift from the null value is given due to the numerical character of the solution preventing the division by zero. This constraint should also prevent another type of flutter instability below the certification speed that may be caused by the design variable changes. The constraint should therefore be applied to all modes included in the solution.

The objective function is defined simply as minimization of pitch and yaw frequency sum as:

$$OBJ=min\left(f_1+f_2\right) \tag{15}$$

As the output, we will obtain the engine pitch and yaw stiffness for which the flutter speed is equal to the specified certification speed and the yaw-to-pitch frequency ratio is equal to specified target value. The optimization is then repeated for a several yaw-to-pitch frequency ratios, typically ranging from 1.05 to 2.0 to get enough points to construct a stability boundary curve. Note that the described solution is applicable for the whirl divergence as well.

The procedure described above is applicable to the "no downwash" option (see section 2). Provided the downwash effects are to be included, the procedure is extended by the extra steps described here. The basic assumption is, that the minor change in the engine pitch and yaw frequencies will have negligible effect on the downwash terms. The downwash terms are therefore calculated only for the structure optimized excluding the downwash as described above. After that, the downwash terms are calculated and the main optimization step is repeated in the same manner as described above.

Due to the possibility of switching of the engine pitch or yaw mode frequency with the other modes, it is worth to re-order the modes at the end of the optimization iteration, provided such mode switch appear. The re-ordering is based on the cross-orthogonality correlation analysis of both sets of modes (before and after the optimization iteration) using the modal assurance criterion, which is expressed as:

$$MAC(\psi_1,\psi_2)=\frac{\left|\left(\{\psi_1\}^t\{\psi_2\}\right)\right|^2}{\left(\{\psi_1\}^t\{\psi_1\}\right)\left(\{\psi_2\}^t\{\psi_2\}\right)} \tag{16}$$

where $\psi_1$ and $\psi_2$ are correlated mode shapes. Only engine pitch or yaw modes are switched, if necessary.

### 6.2 Solution for Full-span Model

The optimization solution for a full-span model is more complicated. We define four design variables: 1) effective stiffness of the engine attachment for symmetric pitch, 2) effective stiffness of the engine attachment for antisymmetric pitch, 3) effective stiffness of the engine attachment for symmetric yaw and 4) effective stiffness of the engine attachment for antisymmetric yaw. These design variables are related to the spring constants of two grounded spring elements ($K_{\delta 1}$ and $K_{\delta 2}$) and to torsional stiffness of two pairs of rod elements [$(GI_k)_1$ and $(GI_k)_2$]. However, the relation is not direct here due to the above mentioned cross-influences (see section 5.2).

We define three frequency ratios: 1) pitch frequency ratio (VFR = $f_{A\Theta}/f_{S\Theta}$), 2) yaw frequency ratio (HFR = $f_{A\Psi}/f_{S\Psi}$) and finally 3) critical frequency ratio (CFR). Critical modes are those ones, the combination of which causes a flutter instability. Choice of the critical modes is dependent on the relation of directions of rotation of both propellers, and on the mode order. Considering the identical directions (i.e., CW-CW or CCW-CCW), the critical modes are symmetric pitch and antisymmetric yaw (it corresponds to a half-span symmetric case) or antisymmetric pitch and symmetric yaw (it corresponds to a half-span antisymmetric case). Considering the inverse directions (i.e., CW-CCW or CCW-CW), the critical modes are symmetric pitch and symmetric yaw or antisymmetric pitch and antisymmetric yaw. Note that CW denotes for the clockwise direction and CCW denotes for the counter-clockwise direction.

VFR and HFR are not changeable. The values are set according the ground vibration test results or guessingly. The typical ratios are ranging from 1.12 to 1.18. CFR is an analogy of TFR shown above.

We assume the typical frequency order (i.e. pitch frequency lower compare to the yaw frequency) in the following description. The first preparatory step is intended to set the initial design variables for the main optimization.

The design constraint includes the requirement to keep the frequency of the selected engine vibration mode, typically the highest one ($f_{A\Psi}$), at the selected value ($f_{A\Psi T}$) using the ±2% band as:

$$ABS\left(\frac{(f_{A\Psi}-f_{A\Psi T})}{f_{A\Psi T}}\right)<0.02 \tag{17}$$

The objective function is defined as the minimization of the frequency ratio error expressed as:

$$OBJ=min\left\{SSQ\left[\left(\frac{f_{A\Theta}}{f_{S\Theta}}-VFR\right),\left(\frac{f_{A\Psi}}{f_{S\Psi}}-HFR\right),\left(\frac{f_{A\Psi}}{f_{S\Theta}}-CFR\right)\right]\right\} \tag{18}$$

or as:

$$OBJ=min\left\{SSQ\left[\left(\frac{f_{A\Theta}}{f_{S\Theta}}-VFR\right),\left(\frac{f_{A\Psi}}{f_{S\Psi}}-HFR\right),\left(\frac{f_{S\Psi}}{f_{S\Theta}}-CFR\right)\right]\right\} \tag{19}$$

where SSQ denotes for sum of squares. Eq. (18) is applicable for the case of identical directions of propeller rotations while eq. (19) is applicable for the case of inverse directions of propeller rotations. This preparatory analysis gives the initial values of design variables for the main optimization. Frequency ratios are equal to VFR, HFR and CFR values.

The main optimization is performed similarly as for the half-span model. The design constraints include the requirement to keep the frequency ratios, again, with the ±2% band as:

$$ABS\left(\frac{\left(\frac{f_{A\Theta}}{f_{S\Theta}}-VFR\right)}{VFR}\right)<0.02 \tag{20}$$

$$ABS\left(\frac{\left(\frac{f_{A\Psi}}{f_{S\Psi}}-HFR\right)}{HFR}\right)<0.02 \tag{21}$$

and

$$ABS\left(\frac{\left(\frac{f_{A\Psi}}{f_{S\Theta}}-CFR\right)}{CFR}\right)<0.02 \tag{22}$$

or

$$ABS\left(\frac{\left(\frac{f_{S\Psi}}{f_{S\Theta}}-CFR\right)}{CFR}\right)<0.02 \tag{23}$$

Again, eq. (22) is applicable for the case of identical directions of propeller rotations while eq. (23) is applicable for the case of inverse directions of propeller rotations.

Another constraint including the requirement to keep the flutter stability (i.e., negative damping) at the selected certification speed $V_{cert}$ is expressed in the same way as for the half-span model, i.e. by eq. (14).

The objective function is defined as minimization of frequency sum, here expressed as:

$$OBJ = min\left[\, SUM\left(f_{S\Theta}, f_{A\Theta}, f_{S\Psi}, f_{A\Psi}\right)\right] \tag{24}$$

As the output, we will obtain the values of design variables ($(K_{\delta 1};\ K_{\delta 2}; (GI_k)_1; (GI_k)_2$), for which the flutter speed is equal to the specified certification speed and three specified frequency ratios are equal to the specified target values. Similarly as for the half-span model, the optimization is then repeated for a several CFR values, typically ranging from 1.05 to 2.0 to get enough points to construct a stability boundary curve. Also, the notes regarding the divergence, downwash effect and regarding the mode switches mentioned in section 6.1 are valid also for the full-span model.

## 7 APPLICATION EXAMPLE

The reference model to test the described methodology was derived from the model of the new Czech twin wing-mounted engine commuter aircraft for 19 passengers with the maximal take-off weight of 7000 kg.

For the purpose of the first test analyses, the simplified model with four degrees-of-freedom, which are represented by both the symmetric and antisymmetric engine pitch and yaw vibrations, was used. Stiffness characteristics of residual structure, which were modeled using beam elements, were replaced by rigid connections and control surface and tab actuation drives were blocked.

Aerodynamic model included only the wing, nacelles and tip tanks. This simplification was made with regard to the fact, that the aerodynamics of the fuselage and tail surfaces has the negligible effect to the whirl flutter phenomenon. Wing was modeled as Doublet-Lattice Panels and nacelles and tip tanks were modeled as Slender and Interference Bodies. The aerodynamic model included also correction factors for the propeller slipstream applied to the appropriate aerodynamic elements of the wing and nacelles. Furthermore, there was also a correction in the aerodynamic forces and moments at the nose part of the control surfaces. The aerodynamic model is shown in figure 7.

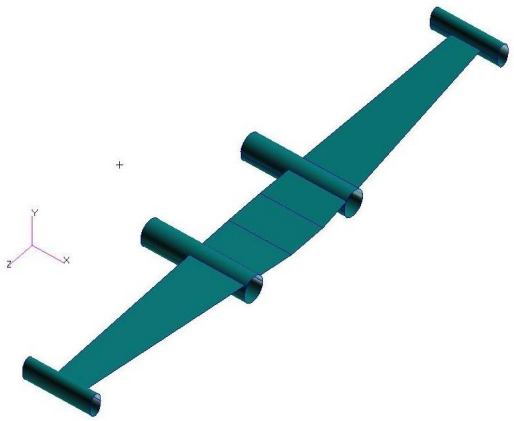

Figure 7. Aerodynamic full-span model of reference aircraft - reduced model (wing, nacelles and tip tanks), only interference tubes are depicted for bodies.

Flight parameters for test analyses were chosen according the aircraft flight envelope. Certification speed was $V_{cert} = 191.4$ m.s$^{-1}$, air density $\rho = 0.7963$ kg.m$^{-3}$ (altitude H = 4267 m) and reference Mach number M = 0.493. Structural damping was neglected. First set of analyses, which is presented here, include the symmetric propeller revolutions, i.e. same revolutions for both left and right propeller ($\Omega = 2080$ rpm). Tested directions of propeller revolutions include CW-CW and CW-CCW combinations.

For the case of identical directions of propeller revolutions (CW-CW), two mechanisms for the whirl flutter appear: 1) a combination of symmetric pitch and antisymmetric yaw modes (SΘ/AΨ) and 2) a combination of antisymmetric pitch and symmetric yaw modes (AΘ/SΨ). The stability margins were calculated with respect to both of the mechanisms of whirl flutter and both are presented in figure 8. As is apparent from the figure, the required engine pitch and yaw frequency is higher for the former mechanism of whirl flutter. Therefore, this mechanism of flutter is more critical compare to the latter one. Values of VFR and HFR were considered at the three levels (1.00; 1.05; 1.10). As the influence of VFR and HFR on the stability margin is negligible, the influence of remaining modes on the stability is negligible as well.

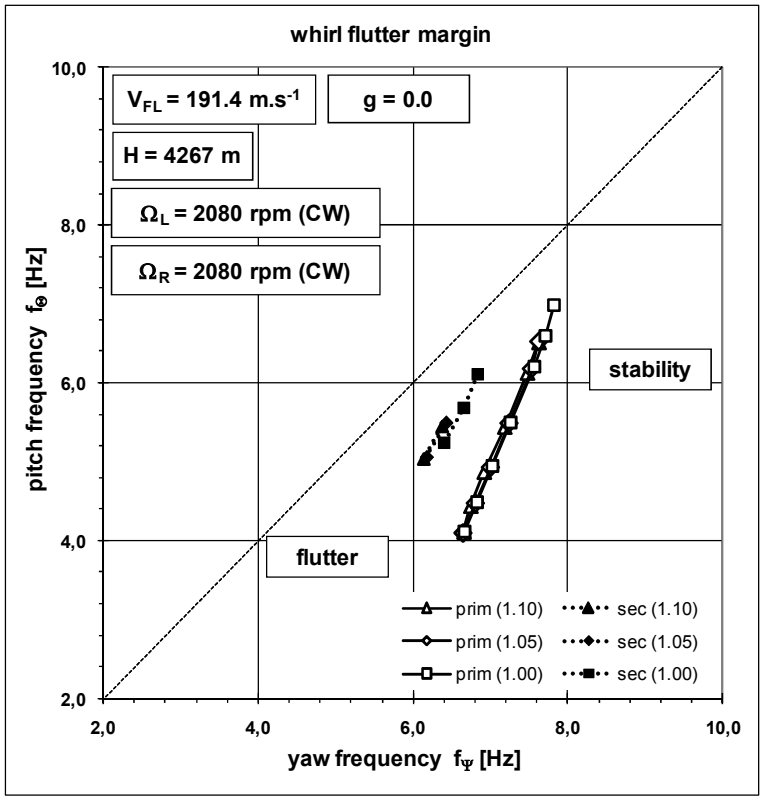


Figure 8. Whirl flutter stability margins - identical directions of revolutions (CW-CW), legend: prim = primary flutter (SΘ/AΨ), sec = secondary flutter (AΘ/SΨ), (1.xx) = VFR, HFR

Figure 9 shows the example of a V-g-f (velocity - damping - frequency) diagram calculated by the standard approach. The crossing of the V-g curve from the negative to the positive damping values represents a flutter state. The mode nr.1 (SΘ mode) crossing represents the primary flutter mechanism (SΘ/AΨ). The flutter speed is here equal to the certification speed. The mode nr.2 (AΘ mode) crossing represents the secondary flutter mechanism (AΘ/SΨ). The flutter speed is here above the certification speed, i.e. above the stability margin, as this type of instability is less critical.

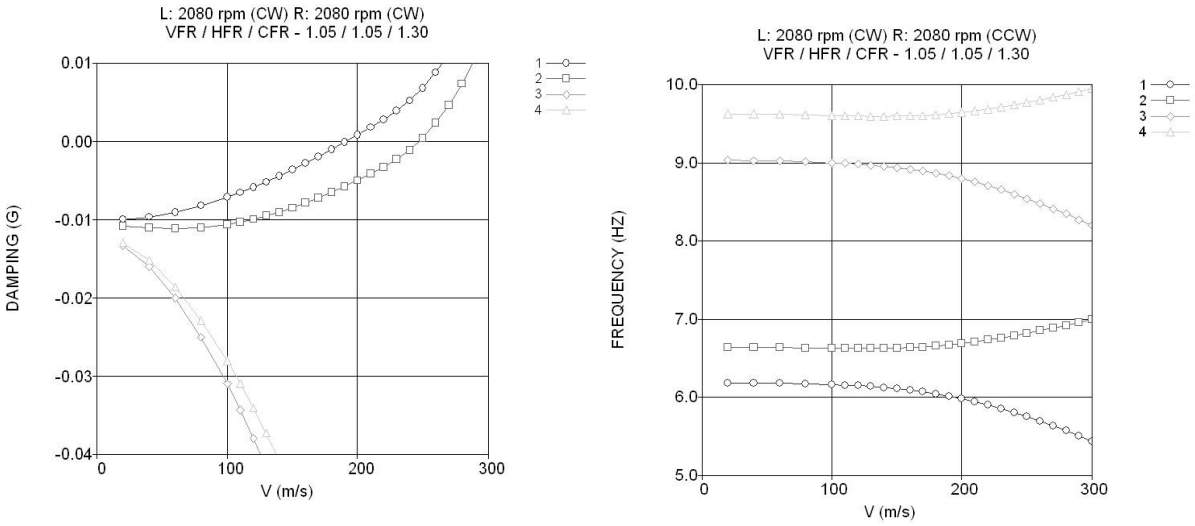


Figure 9. Example of V-g-f diagram - identical directions of revolutions (CW-CW)

For the case of inverse directions of propeller revolutions (CW-CCW), the character of the whirl flutter is different. The instability is caused by the combination of antisymmetric pitch and antisymmetric yaw modes (AΘ/AΨ). Stability margins are presented in figure 10. Compared to the CW-CW case, the required engine pitch and yaw frequencies are considerably higher. Furthermore, this type of instability is influenced also by the remaining modes (SΘ and SΨ) as the influence of VFR and HFR on the stability margin is remarkable.

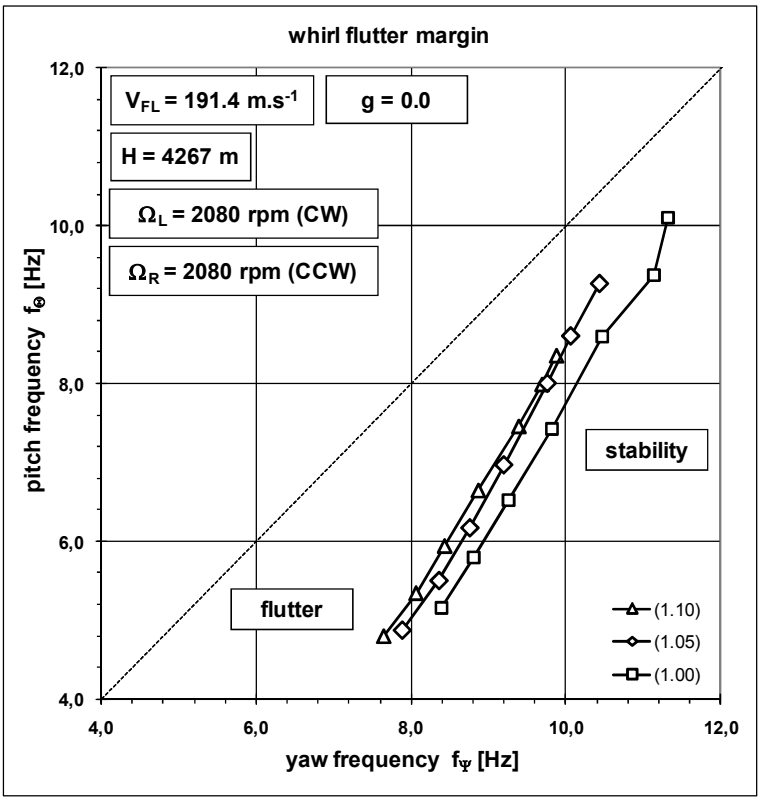


Figure 10. Whirl flutter stability margins - inverse directions of revolutions (CW-CCW), legend: (1.xx) = VFR, HFR

Similarly to the previous case, figure 11 shows the example of a V-g-f diagram for the inverse directions of propeller revolutions. The mode nr.2 (AΘ mode) represent the flutter mechanism (AΘ/AΨ). The flutter speed is here equal to the certification speed.

## 8 CONCLUSION

This paper presents the optimization-based approach to whirl flutter analysis and the application of the method to the full-span model of the aircraft structure. The necessary adjustments of a stick computational model to make it applicable as a full-span and also the modification of the optimization solution are described. The methodology is demonstrated on the reference model of a twin-engine turboprop commuter aircraft. First test analyses including the symmetric propeller revolutions with both available choices of both propeller rotation directions, i.e. CW-CW and CW-CCW are presented. The results include whirl flutter stability margins for several flutter mechanisms. The most critical one is the case of inverse directions of propeller revolutions (CW-CCW), for which, the critical flutter modes are engine antisymmetric pitch and antisymmetric yaw. The future work will be focused on additional choices of propeller rotations, including unsymmetrical revolutions representing the failure cases of a single propeller overspeed, and the absence of a single propeller rotation representing a failure case of a single propeller feathering.

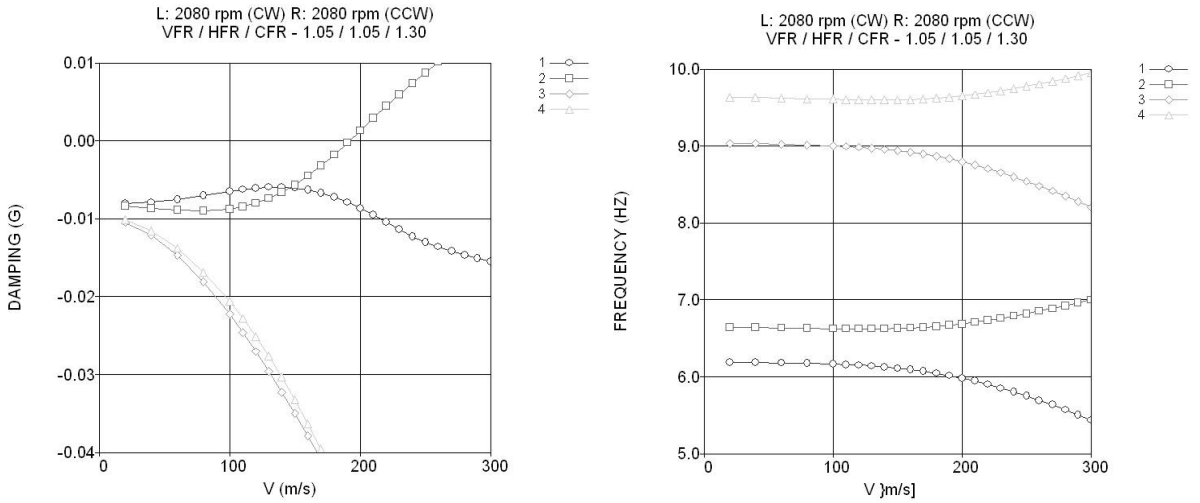


Figure 11. Example of V-g-f diagram - identical directions of revolutions (CW-CCW)

## REFERENCES


[1] *Certification Specifications for Normal, Utility, Aerobatic, and Commuter Category Aeroplanes, CS-23, Amendment 3*, European Aviation Safety Agency, 20.7.2012

[2] *Federal Aviation Regulations, Part 23: Airworthiness Standards: Normal, Utility, Acrobatic and Commuter Category Airplanes, FAR-23, Amendment 62*, US. Department of Transportation, Federal Aviation Administration, 31.1.2012

[3] H.S. Ribner, *Propellers in Yaw*, NACA Report 820, 1945

[4] H.S. Ribner, *Formulas for Propellers in Yaw and charts of the Side – Force Derivatives*, NACA Report 819, 1945

[5] J.C. Houbolt, W.H. Reed, Propeller – Nacelle Whirl Flutter, *Journal of the Aerospace Sciences*, 29, 333 – 346, 1962

[6] H.W. Forsching, *Grundlagen der Aeroelastik*, Springer - Verlag, 1974, ISBN 0387065407, 9780387065403

[7] E.S. Taylor, K.A. Browne, Vibration Isolation of Aircraft Power Plants, *Journal of Aerospace Sciences*, 6 (2), 43-49, 1938

[8] W.H. Reed, R.M. Bennett, Propeller Whirl Flutter Considerations for \V/STOL Aircraft, *CAL/TRECOM Symposium*, Buffalo, NY, USA, 1963

[9] F. Kiessling, Some Problems in Research on Whirl Flutter in V/STOL Aircraft,. *European Space Research Organisation*, ESRO-TT-60, May 1975

[10] J. Cecrdle, *Whirl Flutter of Turboprop Aircraft Structures*, Elsevier Science, 2015, ISBN 978-1-782421-85-6, eISBN 978-1-782421-86-3

[11] T. Theodorsen, *General Theory of Aerodynamic Instability and the Mechanism of Flutter*, NACA Report 496, 1935

[12] J.P. Giessing, T.P. Kalman, W.P. Rodden, Subsonic Steady and Oscillatory Aerodynamics for Multiple Interfering Wings and Bodies, *Journal of Aircraft*, 9, 693-702, 1972

[13] W.P. Rodden, E.D. Bellinger, Aerodynamic Lag Functions, Divergence, and the British Flutter Method, *Journal of Aircraft*, 19, 596-598, 1982

[14] G.J. Moore, *MSC/NASTRAN Design Sensitivity and Optimization*, The MacNeal Schwendler Corporation, Los Angeles, CA, USA, May 1994